Computational Fluid Dynamics Modeling of the Paddle Dissolution Apparatus: Agitation Rate, Mixing Patterns, and Fluid Velocities

Leonard G. McCarthy,[1] Geoff Bradley,[2] James C. Sexton,[2] Owen I. Corrigan,[1] and Anne Marie Healy[1]

[1]School of Pharmacy, University of Dublin, Trinity College Dublin, Ireland
[2]Department of Mathematics and Trinity Centre for High Performance Computing, University of Dublin, Trinity College Dublin, Ireland

ABSTRACT

The purpose of this research was to further investigate the hydrodynamics of the United States Pharmacopeia (USP) paddle dissolution apparatus using a previously generated computational fluid dynamics (CFD) model. The influence of paddle rotational speed on the hydrodynamics in the dissolution vessel was simulated. The maximum velocity magnitude for axial and tangential velocities at different locations in the vessel was found to increase linearly with the paddle rotational speed. Path-lines of fluid mixing, which were examined from a central region at the base of the vessel, did not reveal a region of poor mixing between the upper cylindrical and lower hemispherical volumes, as previously speculated. Considerable differences in the resulting flow patterns were observed for paddle rotational speeds between 25 and 150 rpm. The approximate time required to achieve complete mixing varied between 2 to 5 seconds at 150 rpm and 40 to 60 seconds at 25 rpm, although complete mixing was achievable for each speed examined. An analysis of CFD-generated velocities above the top surface of a cylindrical compact positioned at the base of the vessel, below the center of the rotating paddle, revealed that the fluid in this region was undergoing solid body rotation. An examination of the velocity boundary layers adjacent to the curved surface of the compact revealed large peaks in the shear rates for a region within ~3 mm from the base of the compact, consistent with a 'grooving' effect, which had been previously seen on the surface of compacts following dissolution, associated with a higher dissolution rate in this region.

KEYWORDS: paddle dissolution apparatus, computational fluid dynamics (CFD), hydrodynamics, fluid mixing, fluid velocities

Corresponding Author: Anne Marie Healy, School of Pharmacy, Trinity College Dublin, Dublin 2, Ireland. Tel: 353-1-6081444. Fax: 353-1-6082783. Email: healyam@ tcd.ie.

INTRODUCTION

The dissolution test is a critical test both for setting quality control standards for drug delivery systems to be marketed, and for research in designing dosage forms and setting specifications. The most commonly used dissolution test apparatus for immediate-release products is the paddle dissolution apparatus, known as Apparatus 2. Several reports in the literature have suggested that there is considerable variability, unpredictability and randomness in dissolution profiles using the paddle dissolution apparatus, even for dissolution apparatus calibrator tablets.[1-6] Dissolution of most drugs is diffusion controlled[7] and, consequently, the mass transfer of such drugs in a stirred vessel is dependent on fluid flow, ie, forced convection.[8-10] Many solid dosage forms disintegrate into smaller fragments and particles during the course of the dissolution test, and the particles decrease in size as dissolution proceeds. Most immediate release tablets behave like this. The flow/mixing patterns and dissolution of particulate systems in the paddle dissolution apparatus are likely to vary depending on agitation conditions, particle size, particle size distribution, and particle density.

Kamba et al[11] have recently determined, using a fluid resistance sensor, that there is a considerable change in agitation force intensity toward the base of the dissolution vessel. Alterations in hydrodynamics in the United States Pharmacopeia (USP) paddle dissolution apparatus may significantly affect drug dissolution, and the dissolution rates may change depending on the location of the dissolving substance in the dissolution vessel.[12] The variability in dissolution results may therefore be attributable not only to differences in the dosage forms being tested but also to the variability associated with the test device.

Previous studies, which measured the velocities in the stirred vessel of the dissolution apparatus, provided some insight into the variable hydrodynamics of the systems.[13-15] More recent studies have used computational fluid dynamics (CFD) to further elucidate the complex hydrodynamics in the test vessel.[16,17] These studies have highlighted a possible problem associated with dead zones in the vessel and potential mixing problems at low rotational speeds between the upper and lower halves of the vessel.

An understanding of the changing hydrodynamic conditions in the dissolution vessel with changes in agitation intensity may facilitate appropriate selection of the rotational speed of the paddle for this particular dissolution test apparatus. In a study of the dissolution of acetylsalicylic acid tablets using a paddle-type apparatus, the "beaker method," Levy[18] showed that in vitro/in vivo correlations could be achieved only at an agitation rate of 50 rpm and not when the paddle was rotated at 60 rpm. It should be noted that the beaker method setup is quite different from the hemispheric paddle method. Only limited information on the change in hydrodynamic conditions with paddle rotational speed has been generated to date for the paddle apparatus.[14-16] Scholz et al[19] have recently shown that the USP paddle dissolution apparatus can be used to simulate variations in hydrodynamics in the upper gastrointestinal tract, provided that an appropriate rotational speed is used. Using both coarse and micronised felodipine powder, they concluded that the best agreement of the in vivo and the in vitro data resulted when paddle speeds of 75 rpm and 125 rpm, simulating "fasted" and "fed" state hydrodynamics in vivo respectively, were used.

In the present work the change in CFD-predicted velocities with agitation speed is examined. Mixing patterns within the dissolution vessel are also examined.

It has previously been shown that dissolution rate can vary significantly for different surfaces of the same tablet.[12] The following is a detailed analysis of the fluid velocities adjacent to these surfaces.

MATERIALS AND METHODS

Modeling the USP Apparatus with No Tablet Present

The USP apparatus was modeled using the CFD package Fluent version 5.4.8 (Fluent Inc, Canterra Resource Park, NH), as previously described.[17] Mesh generation was as previously detailed. Meshing boundary layers were introduced, as previously described,[17] allowing the grid to be refined in the regions where velocity and pressure gradients are likely to be steep.

Following grid adaptation, using the hanging node technique previously outlined,[17] Fluent was set up to examine flow at 25, 50, 100, and 150 rpm. The vessel fluid volume was defined as a rotating reference frame with the appropriate angular rotation (eg, 5.236 rad/s for 50 rpm), while the stirrer wall was stationary in the absolute reference frame. The vessel wall was defined as a rotating wall with an angular rotation of 0 rad/s (stationary in the absolute frame).

Determination of Mixing Path-Lines

It is possible to track the flow of "massless particles" throughout the solution domain with the Fluent software package. Effectively, the resulting output is a path-line, tracking the flow of fluid with time from an initial starting point or starting plane. On definition of a starting plane (0.5 mm from the base of the hemispherical vessel), the package was used to track imaginary massless particles from all gridpoints that were intersected with the computational domain by this plane. Massless particles can be defined as the movement of the fluid itself as opposed to the more complex physics of solid particles in motion in a fluid.

Introduction of a Cylindrical Tablet to the Vessel

A cylinder of 13 mm diameter with a height of 8.5 mm was set up at the base of the vessel, and the fluid velocities in the vessel surrounding the stationary compact were modeled as previously described.[17]

RESULTS AND DISCUSSION

The Influence of Paddle Rotational Speed on the Hydrodynamics in the Paddle Dissolution Apparatus

The velocities in a liquid-filled vessel at a paddle speed of 50 rpm have been previously simulated[17] and good agreement has been shown between predicted velocities and those previously obtained using laser Doppler velocity measurements.[12] The same CFD model was used to simulate the hydrodynamics in the paddle apparatus at 25, 50, 100, and 150 rpm. Results of simulated velocities were compared at the various rpm for similar positions in the vessel as those previously analyzed by Bocanegra et al[13] at 50 rpm. Axial and tangential velocities were compared (as radial velocities were of a low magnitude in the body of the vessel). Tangential velocities on a plane 36.1 mm from the base of the vessel ($Z = -0.197$, using the normalized coordinates specified by Bocanegra et al.[13]) at $R = 0.59413$ are presented at various rpm in Figure 1A and axial velocities on a plane 2 mm above the paddle wings ($Z = -0.066$) at $R = 0.594$ are presented at various rpm in Figure 1B.

To examine the effect of the increase in rpm, the peak values at each rpm for the above velocity predictions were examined. The resulting plots of maximum velocity magnitude at each rpm for both planes are shown in Figure 2. A linear increase in the magnitude of both the axial and tangential components of velocity is predicted by the CFD model for various paddle rotational speeds between 25 and 150 rpm ($r^2 \geq 0.995$). Similar behavior was predicted for axial and tangential velocities for various positions in the vessel. Previously it was demonstrated that at 50 rpm, CFD-simulated results for the paddle showed good qualitative agreement with both the tangential and the axial ultrasound-measured

velocities of Diebold and Dressman.[14,15] Diebold and Dressman also found that measured fluid velocities correlated well and in a linear manner with the rotational speed of the paddle, consistent with the CFD-predicted velocities presented here.
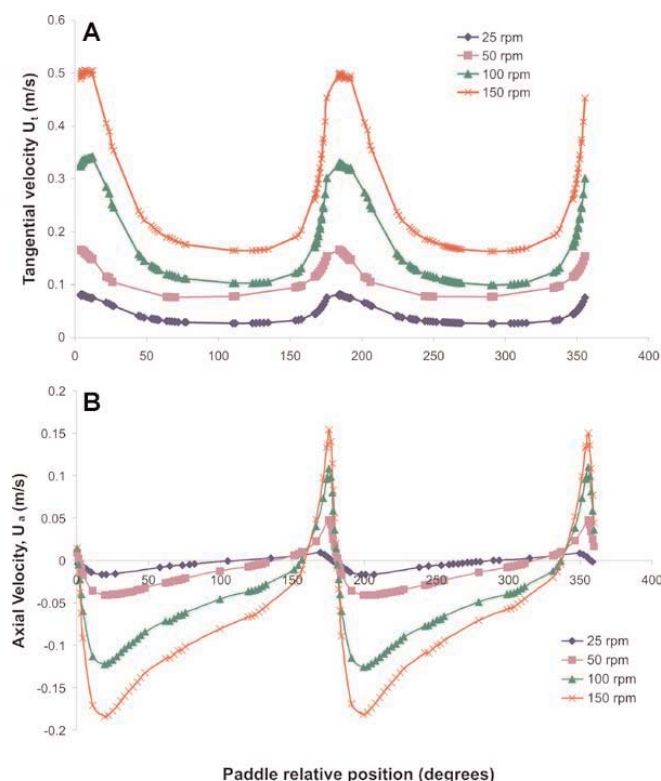

Figure 1. CFD-simulated velocities in the paddle dissolution apparatus vs paddle relative position for paddle rotational speeds of 25, 50, 100, and 150 rpm. (A) tangential velocities (U_t, m/s) at $Z = -0.197$, $R = 0.594$ (Bocanegra et al normalized coordinates, 36.1 mm from the base of the vessel); (B) axial velocities (U_a, m/s) at $Z = -0.066$, $R = 0.594$ (2 mm above the paddle wings).

Mixing Path-Lines in the USP Paddle Apparatus at 50 rpm

An imaginary plane was introduced to the hemisphere of the vessel of the 50-rpm solution at 0.5 mm from the base of the vessel, and the path-lines, which developed from this initial position, were tracked with time. The resulting path-line tracks, from 0.5 seconds to 60 seconds, from a plane 0.5 mm from the very base of the vessel are illustrated in Figure 3. The resulting path-lines provide a novel insight into the 3-dimensional mixing route throughout the USP paddle dissolution apparatus, a feature that has not been possible to deduce from previous velocimetry measurements.[13-15] Initial mixing from the bottom of the vessel wall is facilitated by axial and tangential velocity components, resulting in an upward helical-type flow pattern toward the base of the pad-

dle impeller (0 to 1 second). Convergence with the fluid immediately beside the impeller (5 seconds) imparts significant tangential and radial velocity on the fluid, which results in the movement of the fluid toward the wall of the cylindrical part of the vessel (5 to 10 seconds). Flow from this point onward is predominantly tangential, with a varying degree of positive and negative axial movement, which results in the complete mixing of fluid throughout the vessel (20-40 seconds). Mixing appears also to be suboptimal in the regions immediately inside the vessel walls, in the upper half of the cylindrical volume of the vessel. The previous speculation on poor mixing between zones above and below the paddle[13,16] is not evidenced by the CFD simulations, as the path-lines do not predict a dead-zone of mixing between these 2 regions (at the level of the paddle).
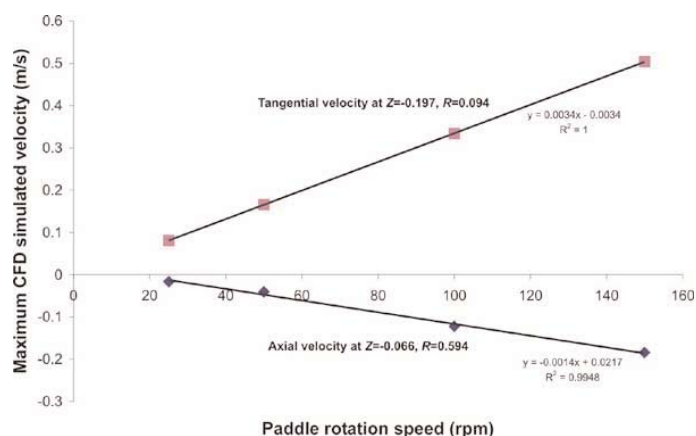

Figure 2. CFD-predicted maximum axial and tangential velocities for 2 positions in the paddle dissolution apparatus for rotational speeds between 25 and 150 rpm. Axial velocities at $Z = -0.066$, $R = 0.594$ and tangential velocities at $Z = -0.197$, $R = 0.094$ (Bocanegra et al normalized coordinates).

Effect of Paddle Rotational Speed on Mixing in the Paddle Dissolution Apparatus

The effect of different paddle speeds on mixing path-lines in the apparatus was examined. Varying the impeller rotational speed had a marked effect on the time required to achieve complete mixing in the apparatus. The term complete mixing is used in a qualitative sense here. The resulting path-lines were examined on various planes over time, until no visual pockets of stagnant liquid were observed. The predicted fluid mixing path-lines in the vessel at various rpm after 5 seconds, from a plane at 0.5 mm from the base of the vessel, are shown in Figure 4.

Using the same grid and solver formulation, quite different flow patterns were predicted for the various rpm, particular-
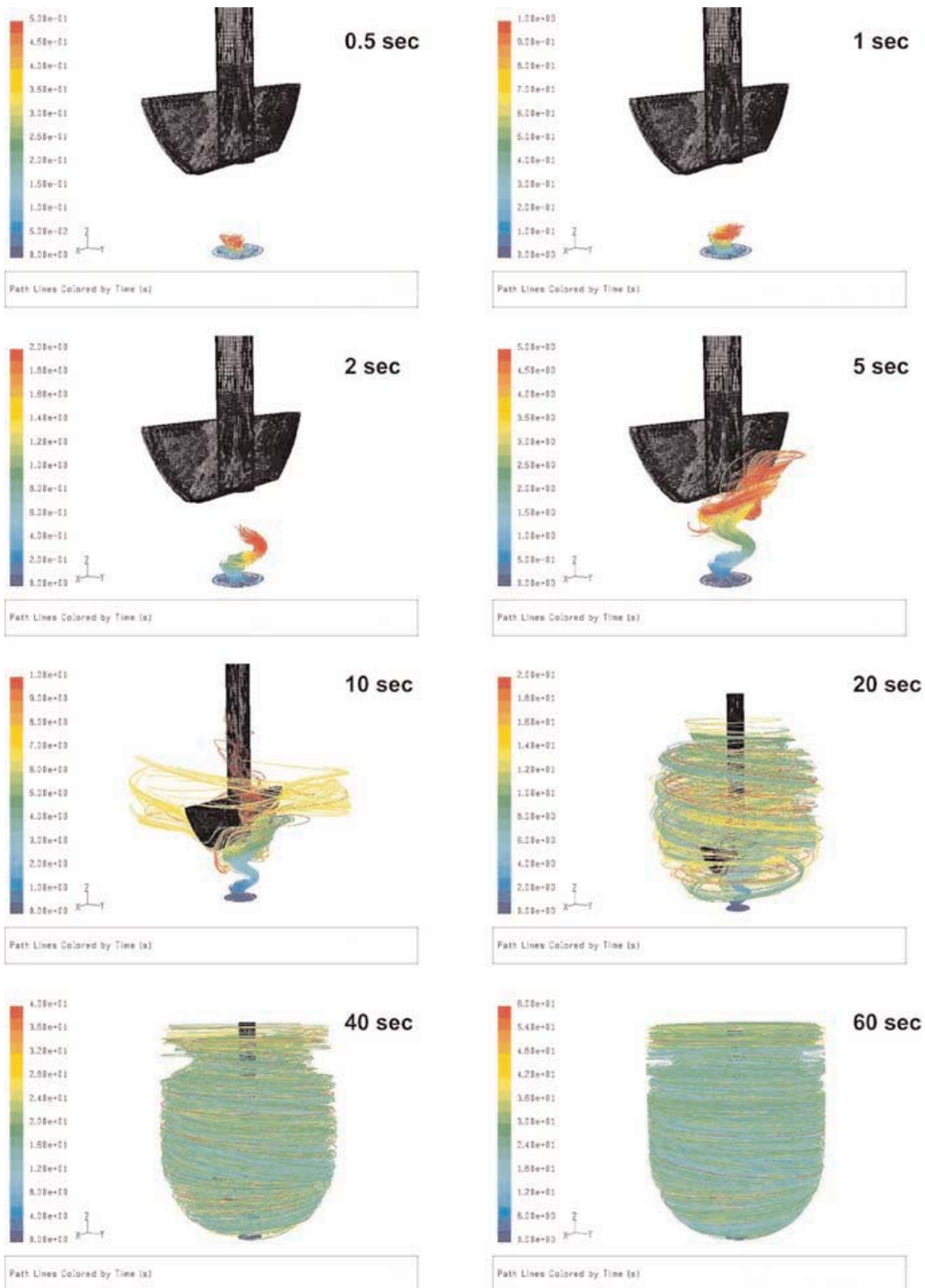
Figure 3. Path-lines of "massless particles" tracked with time over 60 seconds from an initial plane 0.5 mm from the base of the USP paddle dissolution vessel at 50 rpm. Axes are in seconds.
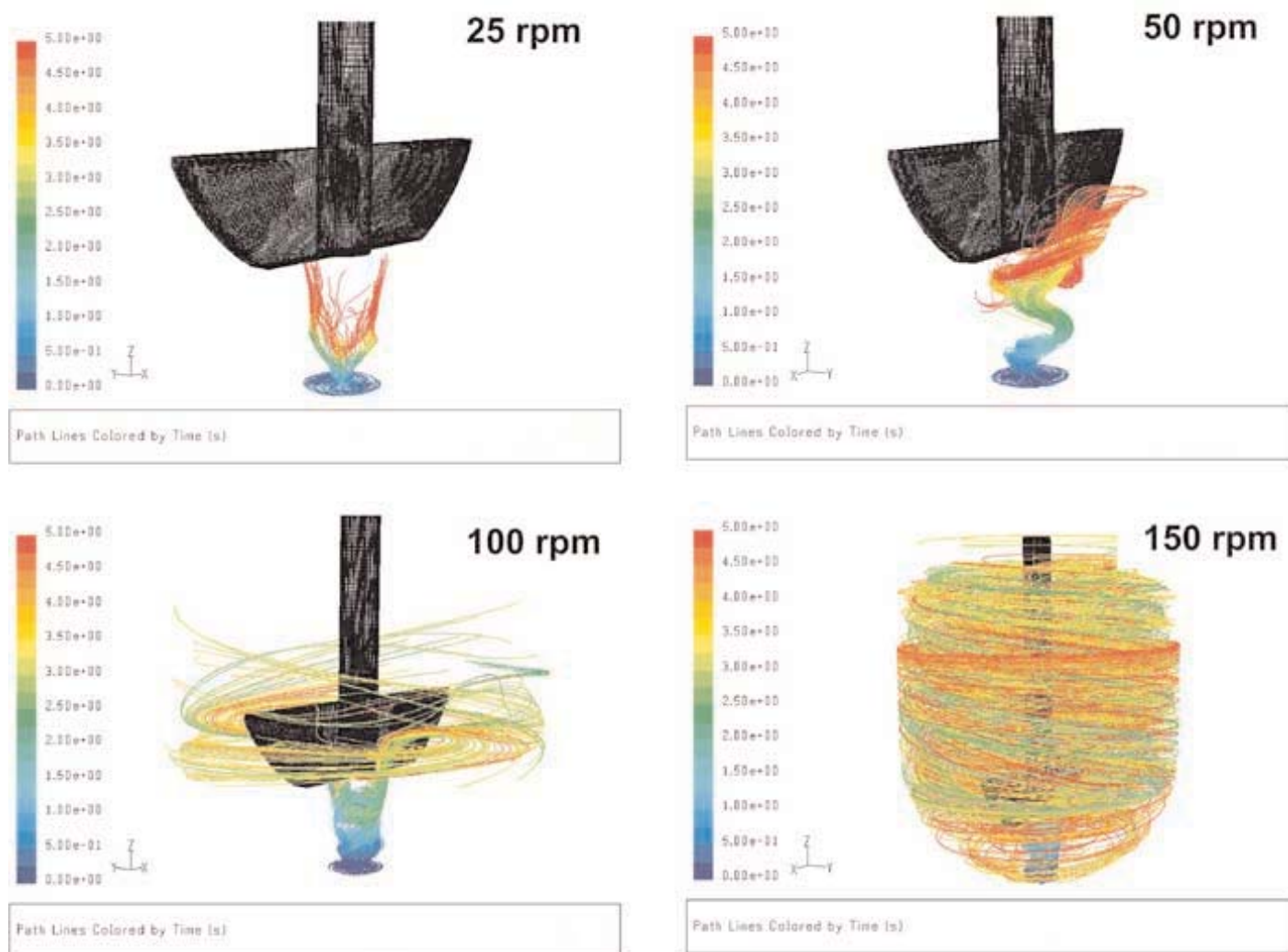
Figure 4. Path-lines of "massless particles" tracked with time for 5 seconds from an initial plane 0.5 mm from the base of the USP paddle dissolution vessel at 25 rpm, 50 rpm, 100 rpm, and 150 rpm. Axes are in seconds (max. 5 seconds in all plots).

ly with regard to the time to allow complete mixing in the vessel. The approximate time required to attain complete mixing from the plane at 0.5 mm from the base of the vessel is 40 to 60 seconds at 25 rpm, 20 to 40 seconds at 50 rpm, 5 to 10 seconds at 100 rpm, and only 2 to 5 seconds at 150 rpm.

Therefore, although complete mixing is predicted by the model, the time to achieve this intimate mixing is quite high at the common operating speeds of 50 and 100 rpm. This suggests that samples taken during the course of a dissolution test at very early time points (> 1 minute) may be quite variable.

Visual Examination of Velocity Boundary Layer on Tablet Surface

The effect on local hydrodynamics of introducing a solid compact/tablet to the base of the dissolution vessel was previously simulated.[17] The presence of the tablet was shown to complicate the local fluid flow, and large fluid shear rates were evident at the base of the compact. Fluid shear rates varied depending on the tablet surface and the location on the surface and were consistent with the reported nonuniform dissolution of model tablets.[12] Examination of the fluid velocities at the surface of the compact revealed that the fluid immediately adjacent to the surface of the compact undergoes a gradual increase from zero velocity to a plateau bulk value over a very small distance.[17] To visually examine the development of this "velocity boundary layer," several 2-dimensional lines were introduced extending from the compact surface into the bulk fluid. The fluid vectors resulting at the intersection between these lines and the individual grid points were examined in closer detail, and the graphical outputs are shown in Figure 5. The development of a velocity boundary layer from the surface of the compact into the fluid is obvious from the lines of selected velocity vectors adjacent to both the curved surface and the upper planar surface. It appears, even on visual inspection, that the thickness of this

velocity boundary layer varies with the surface and location investigated.
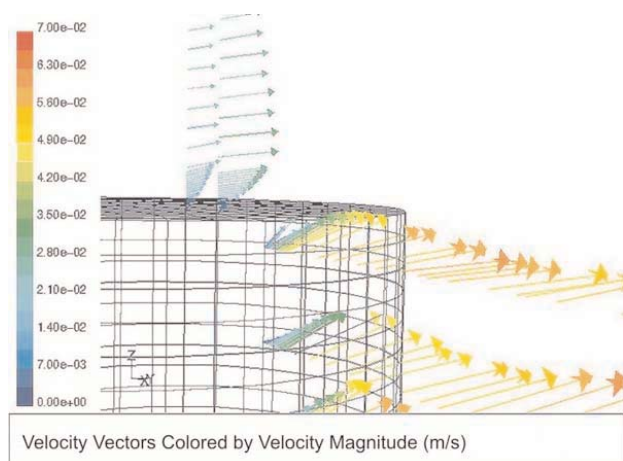

Figure 5. Vectors of velocity magnitude on various lines extending from the compact surface into the fluid, visually indicating the development of a velocity boundary layer in the fluid at the compact surface interface.

Quantitative Analysis of Velocity Boundary Layer at the Tablet Surface

Top Planar Surface

Initially, fluid velocities above the top planar surface were examined. To analyze the magnitude of the velocity boundary layer at this surface, a series of planes in close proximity to the surface of the compact were defined and the tangential component of velocity (parallel to the surface) for such planes was examined in the region directly above the compact.

It was evident that the tangential velocity above the top planar surface of the compact increased with increasing radius. Bocanegra et al[13] and Khoury et al[20] postulated that this feature could be attributable to the fluid undergoing solid body rotation above the compact surface, induced by the solid body rotation of the impeller. If this were the case, the fluid in this region would have a constant angular rotation, ω_f, which would be independent of the radius in this region.

To determine if this was the case, the tangential components of velocity were examined for a series of planes at increasing distance from the top circular surface (over the first 2 mm). It is possible to convert tangential velocities (v_θ) to angular (or rotational) velocities (ω_f), using the equation $v_\theta = \omega_f \cdot r$, where r is the distance from the center point of the paddle (radius). Velocity data for all grid points in a particular plane were determined and the average tangential velocity (over all angles) for a series of radii calculated. The resulting average tangential velocity at each radius was converted to a series of rotational velocities (ω_f) for each radius (40%, 60%, 80%,

and 100% of the compact radius, for each plane). A graded increase in tangential velocity with increasing radius was observed, while the rotational velocities overlapped for all radii examined (with some fluctuation for the lowest radius). The results are indicative of solid body rotation. In order for all the tangential components of flow over the entire plane (compact diameter) to be represented by a single value, the individual values of rotational velocity were averaged for all radii and angles studied. The resulting value, ω_f, for each plane, allows direct comparison of rotational velocities between the planes at various heights.

This process of calculating the average rotational velocity was repeated for a series of planes within a region of high grid refinement at the fluid-compact surface interface. The resulting rotational velocities for the various planes were plotted versus distance from the surface, as shown in Figure 6. (While, as indicated above, data were collected for the top planar surface over 2 mm, the graph obviously levels out well before 2 mm and so data to only 1.5 mm are displayed). The parabolic shape of the profile in Figure 6 represents the development of a velocity boundary layer. The profile reaches a plateau after ~1 mm, where the average rotational velocity remains constant. Therefore, the thickness of the velocity boundary layer for this top planar surface can be said to be in the region of 1 mm.
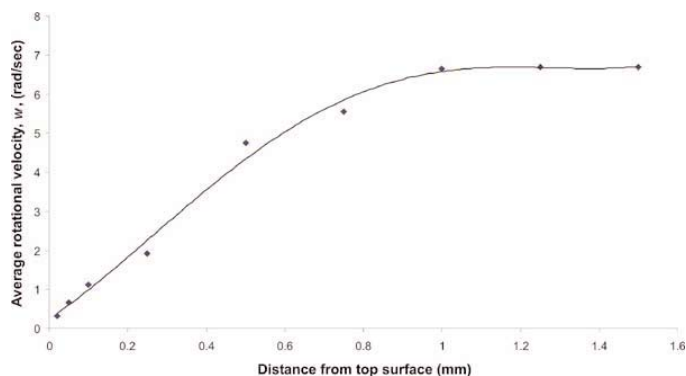

Figure 6. Graph of rotational velocities (ω_f) averaged over all angles for a series of planes (with radius of compact) within 1.5 mm from the top planar surface of the compact at 50 rpm.

Side (Curved) Surface

In order to examine velocities in the fluid adjacent to the curved surface, average values of the relevant velocity component between specified heights were calculated from velocity data for all grid points in "cylinders" surrounding the compact, at various distances from the curved surface. The rotational velocities (ω_f) averaged over all angles between the base and top of the curved surface of the com-

pact for a series of cylinders within 2 mm of the side curved surface of the compact at 50 rpm are shown in Figure 7A.
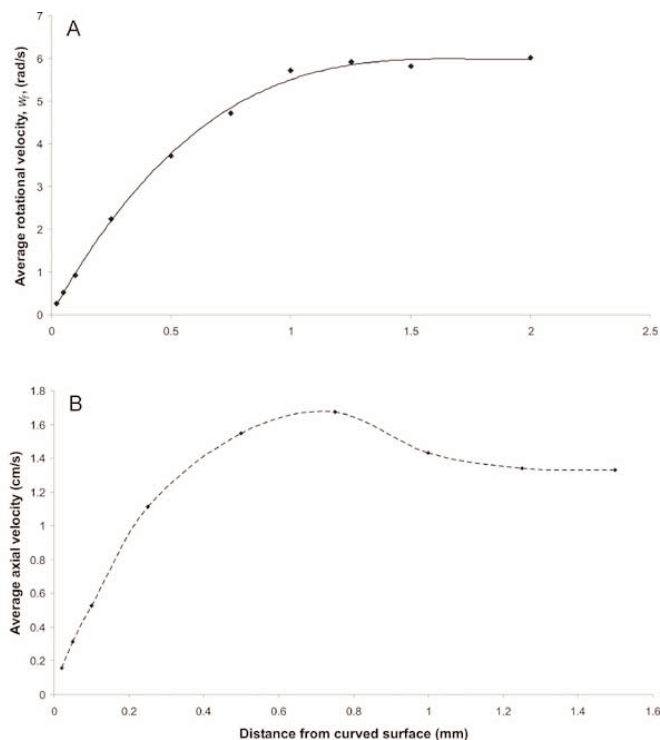

Figure 7. Graph of (A) rotational velocities, ω_f, and (B) axial velocities averaged over all angles from the base of the compact to the top of the curved surface for a series of cylinders within 2 mm from the side curved surface of the compact at 50 rpm.

The velocity boundary layer thickness for the tangential component of velocity can be calculated in this case to ~1.25 mm. It should be noted, however, that all points on the graph of average rotational velocities versus distance for the curved surface (Figure 7A) lie within the error (± 1 standard deviation) of the data shown for the rotational velocities at the top planar surface (Figure 6) and so there is no significant difference in the magnitude of the velocity boundary layers.

A similar evaluation of velocity boundary layer thickness was performed on the average axial component of velocity in the fluid adjacent to the curved surface of the compact; the resulting profile is shown in Figure 7B.

Again, the average axial component of velocity outside the curved surface of the compact attains a value of the bulk at ~1.25 mm. The bulk axial velocity in this region can be approximated as 1.35 cm/s. Although the peak seen before the plateau in Figure 7B seems unusual, such behavior has been mathematically predicted in flow where the surface is stationary with a rotating fluid.[21]

Side (Curved) Surface Subdivisions of Velocity Components

The velocity components in the hydrodynamic boundary layer adjacent to the curved surface of the compact are of particular interest due to the variable dissolution rates that were previously observed for this surface.[12] Therefore, this region was separated into subdivisions, and the resulting fluid velocity components were examined in each subdivision. The cylindrical data in the region next to the curved surface were divided into 6 subdivisions, and the velocity components in each region were treated as outlined in the previous section.

The tangential velocities averaged over all angles for 6 divisions between the base and top of the compact for a series of cylinders within 1.5 mm of the side curved surface of the compact at 50 rpm are shown in Figure 8A. Examination of the rotational velocity produces a more precise output of the shear rates in the velocity boundary layer. The rotational (angular) velocities averaged over all angles for 6 divisions between the base and top of the compact for a series of cylinders within 1.5 mm of the side curved surface of the compact at 50 rpm are shown in Figure 8B. The bulk rotational velocity was higher for the lower 3 mm of the compact, and the thickness of the velocity boundary layer is ~1 mm for all areas adjacent to the curved surface.

The axial velocities, averaged over all angles for 6 divisions between the base and top of the compact for a series of cylinders within 1.5 mm of the side curved surface of the compact at 50 rpm are shown in Figure 9A. Again, a high-velocity region toward the lower base of the compact was evident from the axial velocity profile. The axial velocity component is not as large as the tangential component adjacent to the curved surface.

The radial velocities, averaged over all angles for 6 divisions between the base and top of the compact for a series of cylinders within 1.5 mm of the side curved surface of the compact at 50 rpm are shown in Figure 9B. A region of high inward radial velocity is evident within the lower 1.5 mm adjacent to the curved surface, consistent with the observed preferential erosion of the curved surface toward the base of actual compacts following dissolution.[12,17]

CONCLUSION

Linear increases in velocity magnitude with paddle rotation speed may be predicted for various positions in the vessel of the paddle dissolution apparatus.

At a paddle rotation speed of 50 rpm, path-lines of fluid mixing indicate that mixing between the upper cylindrical and lower hemispherical volumes is not impeded, as previously speculated.[13] However, mixing appears to be suboptimal
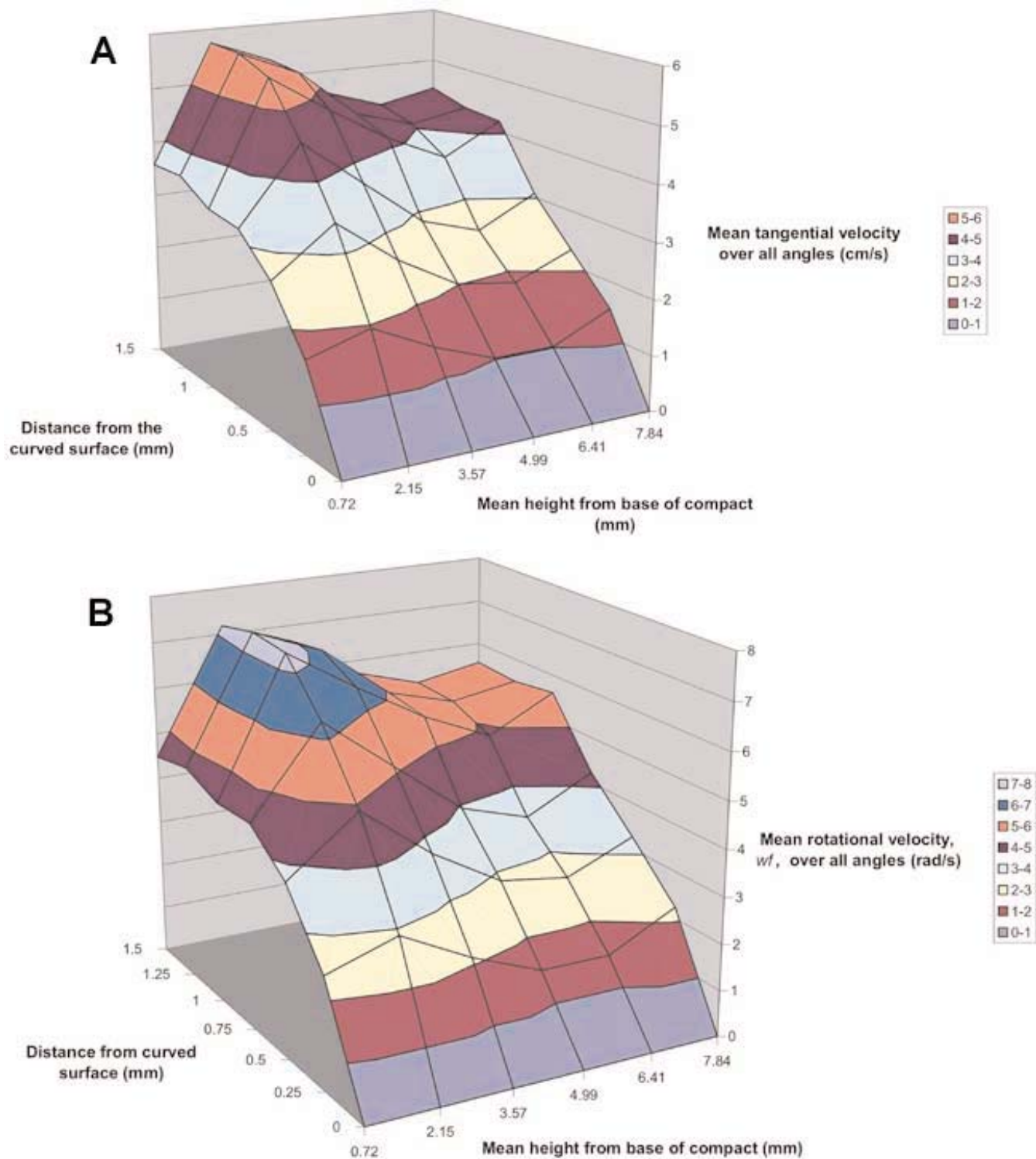
Figure 8. Graph of (A) tangential velocities and (B) rotational velocities, averaged over 6 divisions from the base of the compact to the top of the curved surface, over all angles for a series of cylinders within 1.5 mm from the side curved surface of the compact at 50 rpm.

toward the top of the vessel. The use of different impeller rotational speeds will result in large differences in the time required to achieve complete mixing.

Fluid above the top planar surface of a stationary compact positioned at the base of the vessel undergoes solid body rotation. Fluid flow behavior next to the curved surface is more complex than fluid flow above the upper planar surface. Large peaks in the shear rates for a region within ~3 mm from the base of the compact are consistent with the "grooving" effect, which was seen previously on the surface
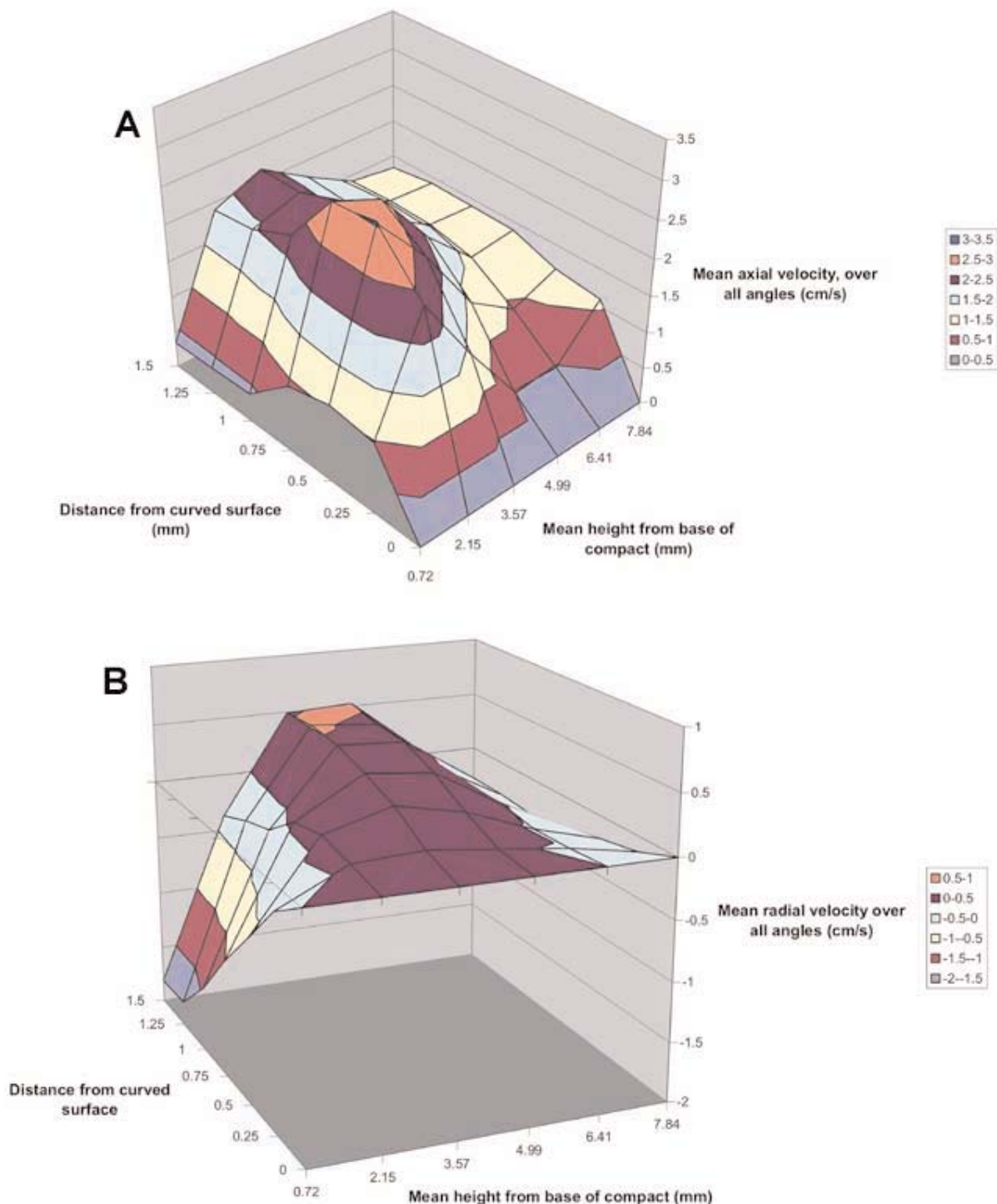
Figure 9. Graph of (A) axial velocity and (B) radial velocity, averaged over 6 divisions from the base of the compact to the top of the curved surface over all angles for a series of cylinders within 1.5 mm from the side curved surface of the compact at 50 rpm.

of compacts following dissolution[12,17] and which was associated with a higher dissolution rate in this region.

Accurate simulations of velocities at different surfaces of a dosage form have potential for allowing a priori prediction of dissolution rates.

REFERENCES

1. Cox DC, Wells CE, Furnam WB, Savage TS, King AC. Systematic error associated with apparatus 2 of the USP dissolution test. II: effects of deviations in vessel curvature from that of a sphere. *J Pharm Sci*. 1982;71:395-399.

2. Gray VA, Hubert BB. Calibration of dissolution apparatus 1 and 2 – What to do when equipment fails. *Pharmacopeial Forum*. 1994;20:8571-8573.

3. Achanta AS, Gray VA, Cecil TL, Grady LT. Evaluation of the performance of prednisone and salicylic acid calibrators. *Drug Dev Ind Pharm*. 1995;21:1171-1182.

4. McCormick TJ. Industry perspective on dissolution apparatus calibration. *Dissolution Technologies*. 1995;2:12-15.

5. Qureshi SA, McGilveray IJ. A critical assessment of the USP dissolution apparatus suitability test criteria. *Drug Dev Ind Pharm*. 1995;21:905-912.

6. Qureshi SA, McGilveray IJ. Typical variability in drug dissolution testing: study with USP and FDA calibrator tablets and a marketed drug (glibenclamide) product. *Eur J Pharm Sci*. 1999;7:249-258.

7. Carstensen JT. Theory of Pharmaceutical Systems, Volume I. London: Academic Press Inc.;1972:238-241.

8. Levich VG. Physicochemical Hydrodynamics. Englewood Cliffs, NJ: Prentice-Hall Inc., 1962.

9. Levich, VG. Theory of concentration polarization. II. Acta Physicochimica U.R.S.S. 1944;19 (2-3):117-132.

10. Grijseels H, Crommelin DJA, de Blaey CJ. Hydrodynamic approach to dissolution rate. *Pharm Weekblad Sci Ed*. 1981;3:129-144.

11. Kamba M, Yasuo S, Takeda N, et al. Measurement of agitation force in dissolution test and mechanical destructive force in disintegration test. *Int J Pharm*. 2003;250:99-109.

12. Healy AM, McCarthy LG, Gallagher KM, Corrigan OI. Sensitivity of dissolution rate to location in the paddle dissolution apparatus. *J Pharm Pharmacol*. 2002;54:441-444.

13. Bocanegra LM, Morris GJ, Jurewicz JT, Mauger JW. Fluid and particle laser Doppler velocity measurements and mass transfer predictions for the USP paddle method dissolution apparatus. *Drug Dev Ind Pharm*. 1990;16:1441-1464.

14. Diebold SM. Hydrodynamik und Lösungsgeschwindigkeit - Untersuchungen zum Einfluss der Hydrodynamik auf die Lösungsgeschwindigkeit schwer wasserlöslicher Arzneistoffe 1. ed., Aachen, Germany:Shaker Verlag; 2000.

15. Diebold SM, Dressman JB. Hydrodynamik kompendialer Lösungsgeschwindigkeits-Testapparaturen. *Pharm Ind*. 2001;63:94-104.

16. Kukura J, Arratia PE, Szalai ES, Muzzio FJ. Engineering tools for understanding the hydrodynamics of dissolution tests. *Drug Dev Ind Pharm*. 2003;29:231-239.

17. McCarthy LG, Kosiol C, Healy AM, Bradley G, Sexton JC, Corrigan OI. Simulating the hydrodynamic conditions in the United States Pharmacopeia paddle dissolution apparatus. *AAPS PharmSciTech*. 2003; 4(2): E22.

18. Levy G, Leonards JR, Procknal JA. Development of in vitro dissolution tests which correlate quantitatively with dissolution rate-limited drug absorption in man. *J Pharm Sci*. 1965;54:1719-1722.

19. Scholz A, Kostewicz E, Abrahamsson B, Dressman JB. Can the USP paddle method be used to represent in-vivo hydrodynamics? *J Pharm Pharmacol*. 2003;55:443-451.

20. Khoury N, Mauger JW, Howard S. Dissolution rate studies from a stationary disk/rotating fluid system. *Pharm Res*. 1988;5:495-500.

21. Schlichting H. Boundary Layer Theory, 4th Edition. New York: McGraw Hill;1979:225-230.